Toxicology Research

PAPER

View Article Online
View Journal | View Issue

Cite this: *Toxicol. Res.*, 2017, **6**, 719

Mitochondrial impairment and oxidative stress mediated apoptosis induced by α-Fe_2O_3 nanoparticles in *Saccharomyces cerevisiae*†

Song Zhu, Fei Luo, Bin Zhu* and Gao-Xue Wang *

Received 28th April 2017,
Accepted 17th July 2017

DOI: 10.1039/c7tx00123a

rsc.li/toxicology-research

In this study, the potential toxicity of α-Fe_2O_3-NPs was investigated using a unicellular eukaryote model, *Saccharomyces cerevisiae* (*S. cerevisiae*). The results showed that cell viability and proliferation were significantly decreased ($p < 0.01$) following exposure to 100–600 mg L^{-1} for 24 h. The IC_{50} and LC_{50} values were 352 and 541 mg L^{-1}, respectively. Toxic effects were attributed to α-Fe_2O_3-NPs rather than iron ions released from the NPs. α-Fe_2O_3-NPs were accumulated in the vacuole and cytoplasm, and the maximum accumulation (3.95 mg g^{-1}) was reached at 12 h. About 48.6% of cells underwent late apoptosis/necrosis at 600 mg L^{-1}, and the mitochondrial transmembrane potential was significantly decreased ($p < 0.01$) at 50–600 mg L^{-1}. Biomarkers of oxidative stress [reactive oxygen species (ROS), superoxide dismutase (SOD), catalase (CAT) and glutathione peroxidase (GPx)] and the expression of apoptosis-related genes (Yca1, Nma111, Nuc1 and SOD) were significantly changed after exposure. These combined results indicated that α-Fe_2O_3-NPs were rapidly internalized in *S. cerevisiae*, and the accumulated NPs induced cell apoptosis mediated by mitochondrial impairment and oxidative stress.

1. Introduction

Due to their distinctive physico-chemical properties, magnetic nanoparticles are being widely used in various fields.[1–3] To date, a wide variety of magnetic nanoparticles have been designed, modified and produced to make them suitable for more commercial applications. As one of the most highly used magnetic nanoparticles, Fe_2O_3 nanoparticles (Fe_2O_3-NPs) have been extensively employed in photocatalysis,[4] lithium storage,[3] sewage treatment[1] and drug delivery.[5] Although Fe_2O_3-NPs show a wide range of applications as well as other benefits, their use is controversial and under much debate.[6,7] Nanoparticles can pass through the cell membrane easily and have relatively greater toxicity than bulk materials due to their nano-size and special properties.[8,9] Therefore, it is imperative to investigate the potential hazards prior to the wide use of Fe_2O_3-NPs. Such knowledge will be useful in the design and modification of Fe_2O_3-NPs and avoiding their potential risks in the future.

In recent years, the potential toxicity of Fe_2O_3-NPs has been evaluated *in vivo*[10,11] and *in vitro*.[6] One of the most accepted mechanisms for the toxicity of nanoparticles is related to oxidative stress that can cause inflammation and apoptosis.[7,11–13] For example, Horie *et al.* (2011) reviewed the cellular responses induced by manufactured nanoparticles and demonstrated that the internalized nanoparticles may affect cells *via* increased reactive oxygen species (ROS) levels followed by dysfunction of mitochondria and apoptosis.[13] Besides, Wu *et al.* (2010) assessed the toxic effects of iron oxide nanoparticles on human cells and reported that nanoparticles were largely internalized by cells through endocytosis, causing eventual cell death possibly by apoptosis.[7] The existing studies mainly focused on rats[11] and the cells of rats and humans;[7] the data about toxicity and the underlying mechanisms of Fe_2O_3-NPs in fungi are currently limited.[14]

Saccharomyces cerevisiae (*S. cerevisiae*) is one of the most studied unicellular eukaryotic model organisms, and has been widely used in molecular and cell biology.[14,15] Its cellular structure, functional organization and metabolic pathways have many similarities to other cells of plants and animals.[16] The genome of *S. cerevisiae* was sequenced in 1996,[17] and 30% of known genes related to human diseases have yeast orthologues.[18,19] Therefore, toxicity studies with *S. cerevisiae* will provide clues to understand toxicity in higher-level organisms, particularly in humans. Importantly, it has a short generation time and can be easily cultured similar to bacteria, making it an ideal model for toxicity assessment. Moreover, *S. cerevisiae* is a widely used eukaryotic model organism for

College of Animal Science and Technology, Northwest A&F University, Yangling 712100, China. E-mail: zhubin1227@126.com, wanggaoxue@126.com; Fax: +86 29 87092102; Tel: +86 29 87092102

†Electronic supplementary information (ESI) available. See DOI: 10.1039/c7tx00123a

the study of oxidative stress and apoptosis, thus lots of data are available for mechanistic studies.[20–22] In recent years, *S. cerevisiae* is increasingly used in the toxicological evaluation of nanoparticles, such as ZnO, CuO, Mn_2O_3 and TiO_2.[8,14,23] In addition, we have investigated the effects of multi-walled carbon nanotubes (MWCNTs) on *S. cerevisiae* and verified that *S. cerevisiae* undergoes apoptosis by the mitochondrial impairment pathway following exposure.[24]

In this study, *S. cerevisiae* was used as an experimental model for investigating the toxicity and underlying mechanisms of α-Fe_2O_3-NPs. Based on previous studies, we hypothesized that (1) cell proliferation and viability would be significantly decreased; (2) the effects would be attributed to α-Fe_2O_3-NPs rather than iron ions released from the NPs; (3) α-Fe_2O_3-NPs would be internalized in *S. cerevisiae*; and (4) cells would be undergoing apoptosis mediated by mitochondrial impairment and oxidative stress. This study contributes to a better understanding of the α-Fe_2O_3-NP toxicity, and lays the foundation for managing risks in the future.

2. Materials and methods

2.1 Characterization of α-Fe_2O_3-NPs

The α-Fe_2O_3-NPs used in this study were purchased from Beijing Dk Nano technology Co., Ltd, (Beijing, China), and their structural parameters are listed in Table S1.† A Hitachi S-4800 scanning electron microscope (SEM; operating at 15 kV) and JEM-1200EX transmission electron microscope (TEM, operating at 100 kV) were used to observe the morphology and size of the α-Fe_2O_3-NPs. Fourier transform infrared spectrometry (FTIR; Bruker Vetex70, Germany) was conducted to record the spectra from 400 to 4000 cm^{-1} using the KBr pellet technique.[25] X-ray diffraction (XRD) patterns were collected on a Bruker D8 Advance diffractometer (Germany) with CuKα radiation (λ = 1.54060 Å) operating at 40 kV and 100 mA. The α-Fe_2O_3-NPs were scanned from 10° to 80° (2θ) with a scanning rate of 1° min^{-1}, and diffraction peaks were compared with those of standard compounds listed in the JCPDS data file. In order to measure elemental compositions and chemical states, X-ray photoelectron spectroscopy (XPS; PHI-5600, Russia) was used. To assess Fe^{3+} released from α-Fe_2O_3-NPs, the suspensions were centrifuged at 12 000 rpm for 30 min to pellet α-Fe_2O_3-NPs. Then, the supernatants were passed through an ultra-filtration filter with a molecular cutoff of 3000 Da. The ferric content in supernatants was then determined using inductively coupled plasma mass spectrometry (ICP-MS, Jarrell-Ash, MA). Dynamic light scattering (DLS, Brookhaven BI-200SM, USA) was used to estimate the hydrodynamic size distribution of α-Fe_2O_3-NPs.

2.2 Toxicity testing

α-Fe_2O_3-NPs were suspended in YPD medium (1% yeast extract, 2% peptone and 2% glucose) to create suspensions with concentrations as required (0, 25, 50, 100, 200, 400 and 600 mg L^{-1}). To evaluate the contribution of Fe^{3+} released from NPs to the toxicity, the suspensions were centrifuged at 12 000 rpm for 30 min and then filtered with an ultra-filtration filter, and the filtrates were collected. *S. cerevisiae* was respectively cultivated in the α-Fe_2O_3-NP suspensions and filtrates with constant shaking at 160 rpm at 30 °C, and the inoculation quantity was approximately 1×10^5 cells per ml. For proliferation assays, cells were counted under an optical microscope (Olympus Optical Co., Ltd, Tokyo, Japan) at 0, 3, 6, 9, 12, 15, 18, 21 and 24 h. For mortality evaluation, cells were collected and stained with 1 mg mL^{-1} Trypan Blue (Sigma, USA) for 3–5 min. The stained cells were checked using the microscope, and the mortality rate was calculated as a ratio between stained cells and total cells.

2.3 Uptake of α-Fe_2O_3-NPs

The uptake of α-Fe_2O_3-NPs by *S. cerevisiae* was observed using a TEM (JEOL, Tokyo, Japan) according to Bayat *et al.*, (2014).[23] In order to quantitatively assess the uptake, cells were collected using density gradient centrifugation[24,26] at 5, 15 and 30 min and 1, 3, 6, 9, 12, 15, 18, 21 and 24 h after exposure to 50 mg L^{-1}. Cells were thoroughly washed with cold phosphate buffer solution (PBS; pH = 7.1) and dried using a freeze dryer (FD5-3, GOLD-SIM). The dried cells (0.1 g) were digested in trace metal grade nitric acid at 160 °C, and then diluted to 5 mL with deionized water. The ferric contents were measured using an ICP-MS (Jarrell-Ash, MA).

2.4 Apoptosis assay

Early apoptosis and late apoptosis/necrosis were checked using annexin V/PI (Beyotime Biotech, Nantong, China) staining.[27,28] Briefly, approximately 1–2 × 10^5 cells were collected after exposure for 24 h, and then stained with annexin-V-FITC (5 μL) and PI (5 μL) following the manufacturer's instruction. After staining, flow cytometry (Beckman Coulter Inc., United States) analysis was immediately conducted. FITC fluorescence (FL1) and PI fluorescence (FL2) of each cell were quantitated using the Cell Quest Pro® software (BD, Germany).

2.5 Detection of mitochondrial transmembrane potential

The mitochondrial transmembrane potential (MTP, $\Delta\psi_m$) was detected using JC-1 (Beyotime Biotech, Nantong, China) as described in previous studies.[29,30] In healthy cells, JC-1 is concentrated in the mitochondria and exists as aggregates (red fluorescence). Upon the MTP decrease, JC-1 is released into the cytoplasm where it fluoresces green as a monomer.[29,30] Therefore, the ratio between red and green fluorescence can indicate the change of MTP. Briefly, cells were separated using density gradient centrifugation after exposure for 24 h and thoroughly washed with cold PBS. Then cells were incubated with JC-1 following the manufacturer's instruction. After staining, cells were analyzed using a fluorescence stereomicroscope (Leica MZFL III, Germany) and a microplate reader (Multiskan MK3, Thermo Labsystems Co., Beverly, MA) with excitation and emission at 514/585 and 530/590 nm, respectively. The ratios between red and green fluorescence were calculated.

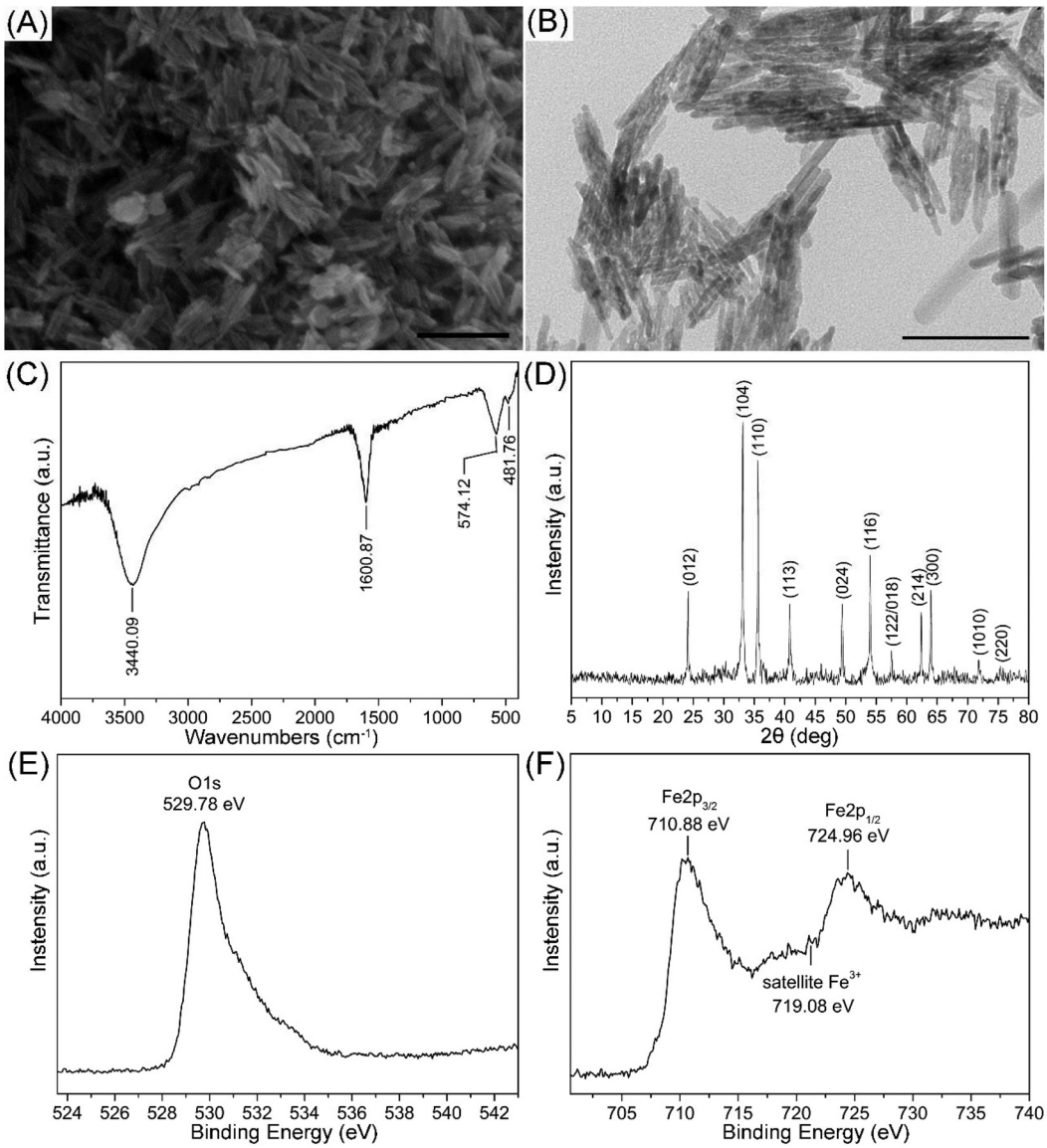

Fig. 1 Characterization of α-Fe_2O_3-NPs. SEM image (A), TEM image (B), FTIR spectrum (C), XRD pattern (D) and XPS spectra (E and F) of α-Fe_2O_3-NPs. Scale bars in A and B are 200 and 100 nm, respectively.

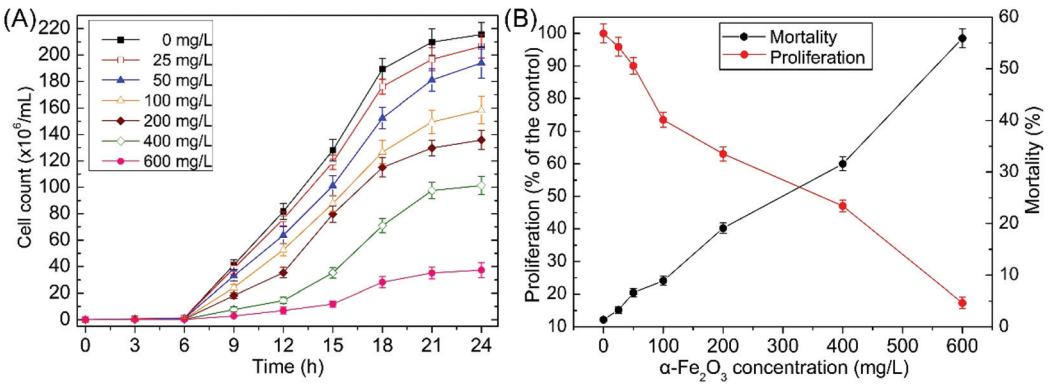

Fig. 2 (A) Growth curves of *S. cerevisiae* exposed to 0–600 mg L^{-1} α-Fe_2O_3-NP suspensions. (B) Effects of α-Fe_2O_3-NPs on cell proliferation and viability after exposure for 24 h. Values are presented as mean ± SD.

2.6 ROS and antioxidant enzyme activities

After exposure for 24 h, approximately 1×10^8 cells were collected from each treatment. The cells were mixed with glass beads (0.3–0.4 mm) and thoroughly ruptured by vigorous vortexing for 5–10 min. After vortexing, the homogenates were centrifuged (12 000 rpm, 4 °C) for 10 min and the supernatants were collected for ROS and antioxidant enzyme activity measurements. A DCFH-DA kit (Beyotime Biotech, Nantong, China) was used for ROS detection. Total protein, superoxide dismutase (SOD), catalase (CAT) and glutathione peroxidase (GPx) activities were measured using kits (Nanjing Jiancheng Bioengineering Institute, Nanjing, China) according to the manufacturer's instructions. ROS and antioxidant enzyme activities were detected by using a microplate reader (Multiskan MK3, Thermo Labsystems Co., Beverly, MA). ROS was also analyzed using a fluorescence microscope (Leica MZFL III, Germany) with excitation at 480 nm and emission at 530 nm.

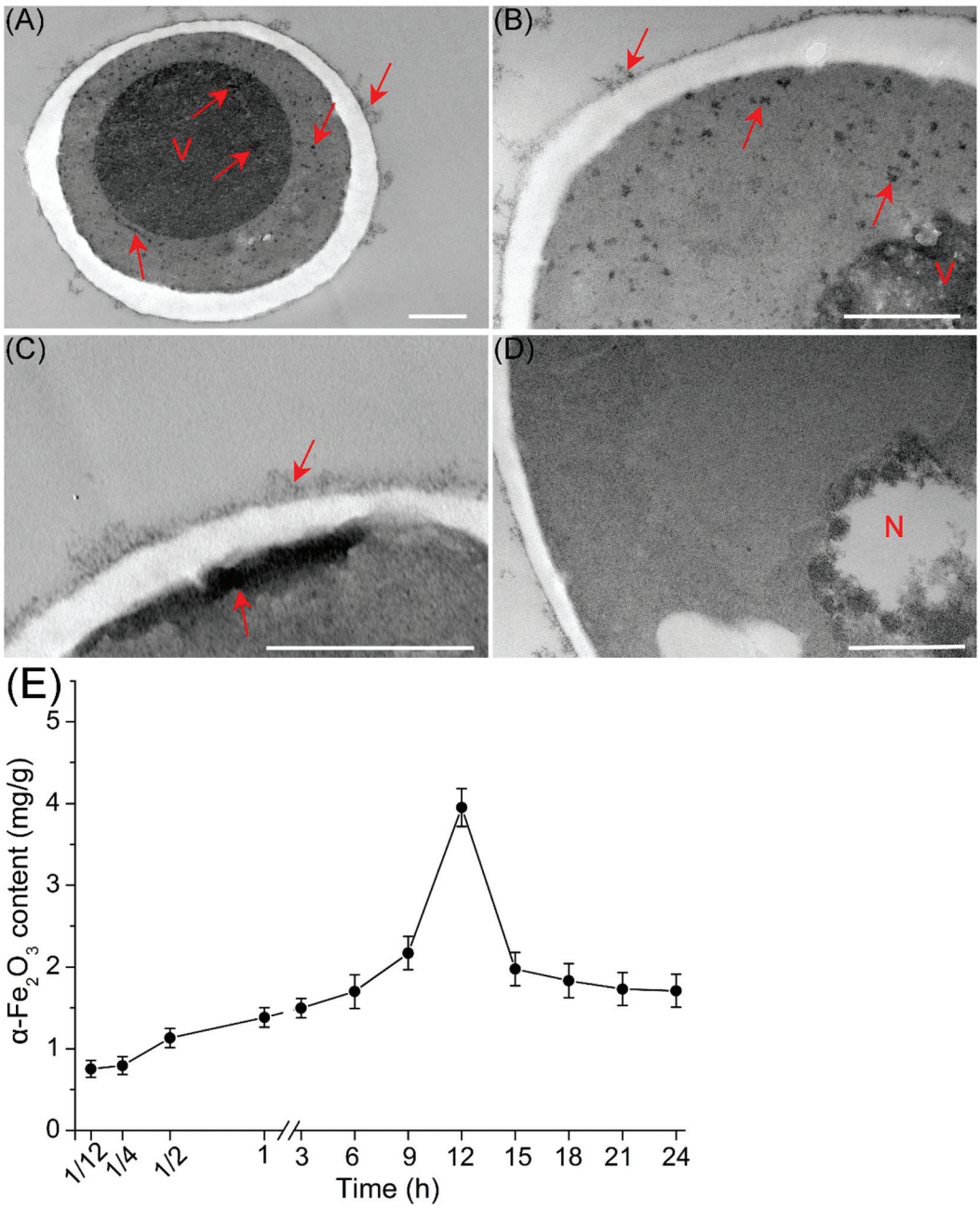

Fig. 3 Uptake of α-Fe_2O_3-NPs and the potential damage to *S. cerevisiae* checked using TEM. (A–C) α-Fe_2O_3-NPs (red arrows) adsorbed on the cell wall and electron dense black deposits were visible inside the cytoplasm and vacuole. (D) Chromatin was condensed along the nuclear envelope. V, vacuole; N, nucleus. Scale bars: 500 nm. (E) Contents of α-Fe_2O_3-NPs uptake by *S. cerevisiae* cells at different time points. Values are presented as mean ± SD.

2.7 mRNA expression assays

Expression of apoptosis-related genes (SOD, Yca1, Nma111 and Nuc1) was measured using real-time PCR (as described in the ESI file†). Primers for the genes and 18S rRNA were designed as per previous studies[24,31] and are listed in Table S2.†

2.8 Statistical analysis

Data were expressed as mean ± standard deviation (SD) for at least three independent experiments. The IC_{50} and LC_{50} values and related 95% confidence limits were calculated using the Probit method. Data were analyzed using SPSS Version 11.0 software package (SPSS Inc., Chicago, IL). Differences between the controls and treatments were analyzed using one-way ANOVA followed by Tukey's test, where $p < 0.05$ was considered significant.

3. Results and discussion

3.1 Characterization of α-Fe_2O_3-NPs

Data showed that the physicochemical properties of nanoparticles have profound impacts on their uptake and toxicity, such as the size, shape and dissolution of nanoparticles.[8,32,33] As shown in the SEM (Fig. 1A) and TEM (Fig. 1B) images, α-Fe_2O_3-NPs were rod-like with varying lengths. The average length was 63.3 nm and smaller than that estimated by DLS (5.2 μm; Table S1†), indicating that α-Fe_2O_3-NPs were rapidly aggregated in the YPD medium. However, the DLS data cannot reveal the real sizes due to the rod-like morphology. The FTIR spectrum of α-Fe_2O_3-NPs is shown in Fig. 1C, the absorption peaks at 3440.09 and 1600.87 cm^{-1} were related to the O–H stretching vibrations, and the bands at 574.12 and 481.76 were due to the Fe–O stretching vibrational modes.[34] The diffraction peaks of α-Fe_2O_3-NPs (Fig. 1D) were in accordance with the standard XRD card of hexagonal α-Fe_2O_3 (JCPDS no. 33-664).[35] The peaks are sharp and no characteristic peaks of impurities can be observed, indicating that the α-Fe_2O_3-NPs are well-crystallized and of high purity. The XPS spectra of α-Fe_2O_3-NPs are shown in Fig. 1E (O 1s) and Fig. 1F (Fe 2p). The photoelectron peaks at 710.88 and 724.96 eV were the characteristic doublets of the Fe $2p_{3/2}$ and $2p_{1/2}$ core-level spectra of iron oxide, respectively. The corresponding satellite peak located at 719.08 eV was attributed to the presence of Fe^{3+} in α-Fe_2O_3-NPs.[36] Contents of Fe^{3+} released from α-Fe_2O_3-NPs were measured, and the result is shown in Table S3.† The contents ranged from 1.54 to 4.81 mg L^{-1}, indicating that only a small amount of NPs was dissolved.

3.2 Cell proliferation and viability

Cell proliferation showed a dose-dependent inhibition (Fig. 2A), and was significantly inhibited ($p < 0.01$) at 100–600 mg L^{-1} after exposure for 24 h (Fig. 2B). The IC_{50} value (inhibition of growth by 50%) was 352 mg L^{-1} (Table S4†). Corresponding to the proliferation, mortality was notably increased ($p < 0.01$) at 50–600 mg L^{-1}. The mortality rate was 56% after exposure to 600 mg L^{-1} for 24 h, and the LC_{50} value was 541 mg L^{-1} (Table S4†). Otero-González *et al.* (2013) investigated the toxicity of some nanoparticles to *S. cerevisiae* and demonstrated that Fe_2O_3-NPs caused no toxicity even at 1000 mg L^{-1}.[14] The obvious disagreement may be induced by the different shape of Fe_2O_3-NPs.[33] Lee *et al.* (2014) reported that the shape of Fe_2O_3-NPs is a major factor that contributes to particle toxicity. They also showed that rod-shaped Fe_2O_3-NPs caused more ROS production and a much higher extent of necrosis compared with other Fe_2O_3 particles.[33] The α-Fe_2O_3-NPs used in this study were rod-like, while they were granular in the previous study.[14] Therefore, higher toxicity was shown in our study.

Metal ions from the dissolution of the nanoparticles may play a key role in the toxic effects of NPs. Kasemets *et al.* (2009) demonstrated that the toxicity of CuO-NPs to *S. cerevisiae* was due to the dissolution of copper ions from CuO.[8] In this study, the contribution of iron ions from the dissolution of NPs to the toxicity was evaluated. As shown in Fig. S1A and B,† there were no significant effects ($p > 0.05$) on cell viability and proliferation, indicating that the toxicity is attributed to α-Fe_2O_3-NPs rather than Fe^{3+} released from the NPs.

3.3 Uptake of α-Fe_2O_3-NPs

TEM is an effective tool to assess the uptake and toxicity of nanoparticles in cellular systems.[23] In this study, the uptake of α-Fe_2O_3-NPs and the potential damage to *S. cerevisiae* were studied using TEM. As shown in Fig. 3, α-Fe_2O_3-NPs adsorbed on the cell wall and electron dense black deposits were visible inside the cytoplasm and vacuole (Fig. 3A–C). The black deposits were internalized NPs or Fe ions.[23] Due to the small amount of Fe ions detected by ICP-MS, the deposits were most likely α-Fe_2O_3-NPs. Chromatin condensation along the nuclear envelope is clearly visible in Fig. 3D. This phenomenon is a typical marker of apoptosis,[27] indicating that cells may

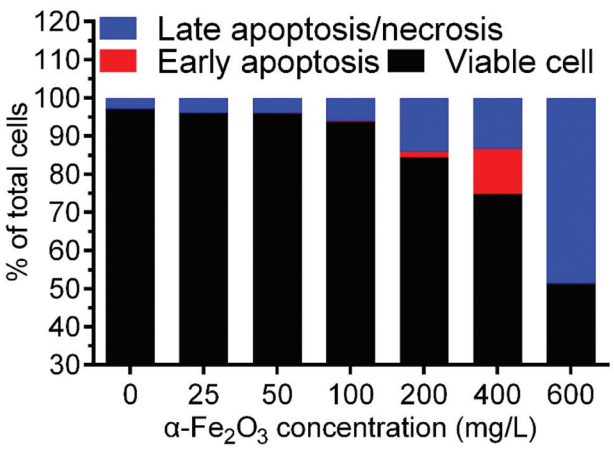

Fig. 4 Percentage of viable, early apoptosis and late apoptosis/necrosis cells after exposure to 0–600 mg L^{-1} α-Fe_2O_3-NP suspensions for 24 h.

undergo apoptosis after exposure to α-Fe_2O_3-NPs. A similar result was reported by Lee *et al.* in 2014, who demonstrated that rod-shaped Fe_2O_3 NPs were found around vacuoles and throughout the cytoplasm of RAW 264.7 cells and induced the nuclei to condense and shrink.[33]

Contents of Fe_2O_3 internalized in *S. cerevisiae* were quantitatively measured by ICP-MS. In order to minimize the adsorption of α-Fe_2O_3-NPs on the cell wall, density gradient centrifugation was performed to separate the cells from NPs.[24,26] As shown in Fig. 3E, the contents showed an increase during the first 12 h followed by a decrease from 12 to 24 h with a range of 0.753 to 3.95 mg g^{-1}. The result indicated that α-Fe_2O_3-NPs were rapidly internalized in *S. cerevisiae* following exposure for 5 min. The decrease is probably due to the discharge of α-Fe_2O_3-NPs. Furthermore, the decrease was slow from 18 to 24 h, indicating that a balance may be achieved between accumulation and elimination.

3.4 Apoptosis of cells

As described above, a typical marker of apoptosis (chromatin condensation) was observed. In order to confirm whether cells underwent apoptosis following exposure to α-Fe_2O_3-NPs, annexin V/PI staining was performed. As shown in Fig. 4, early

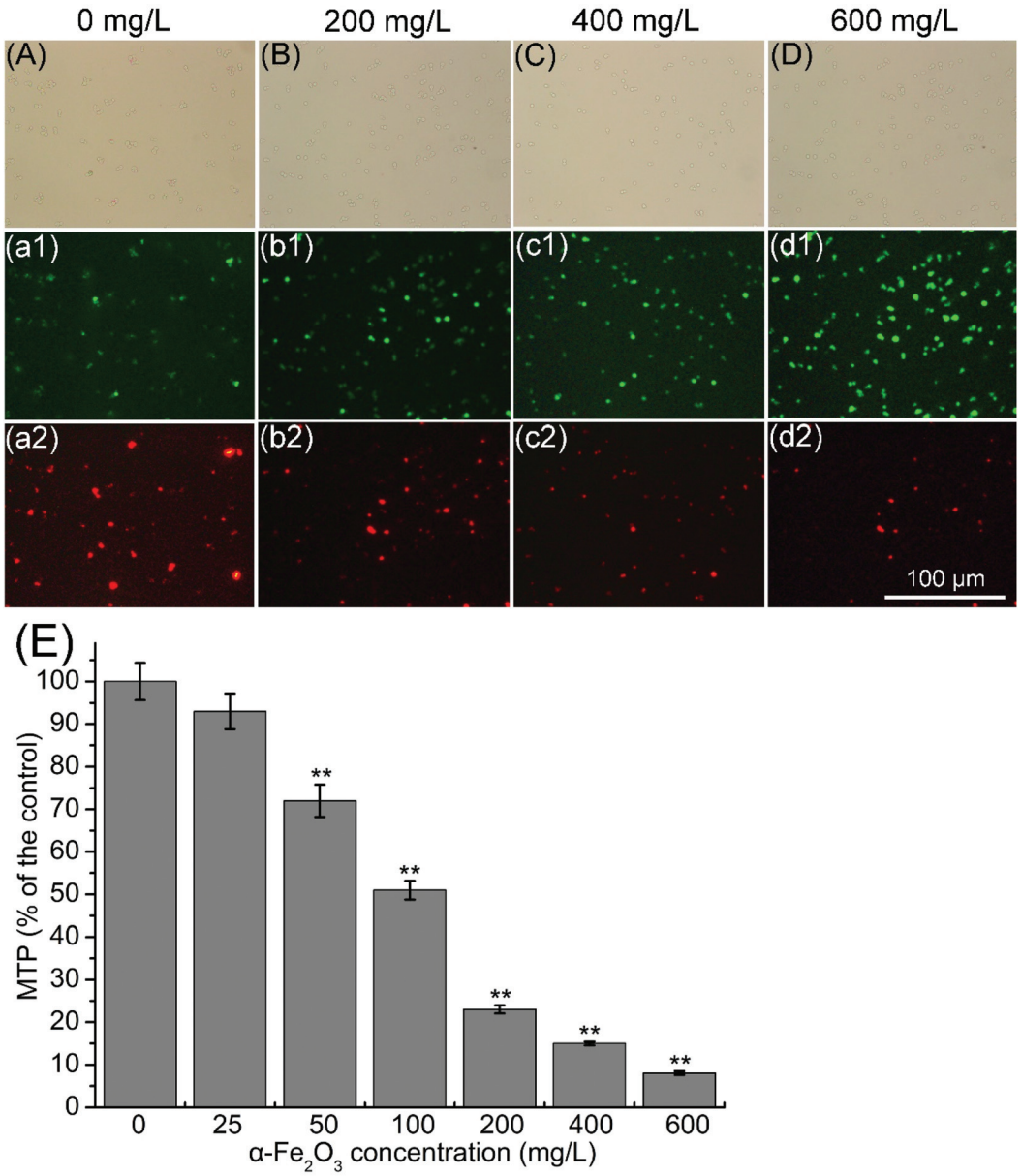

Fig. 5 Mitochondrial transmembrane potential (MTP) of *S. cerevisiae* cells was evaluated using JC-1. MTP of cells exposed to 0 (A, a1 and a2), 200 (B, b1 and b2), 400 (C, c1 and c2) and 600 (D, d1 and d2) mg L^{-1} α-Fe_2O_3-NP suspensions, and measured by using a fluorescence stereomicroscope. (E) MTP of cells exposed to 0–600 mg L^{-1}, and measured by using a microplate reader. Values are presented as mean ± SD. Values that are significantly different from the control are indicated by asterisks (one-way ANOVA, $^{**}p < 0.01$).

apoptosis was markedly increased ($p < 0.01$) only at 400 mg L^{-1} (11.97%) compared with the control (0.02%). For late apoptosis/necrosis, it was significantly increased ($p < 0.01$) at 200–600 mg L^{-1}. At 600 mg L^{-1}, 48.60% of cells underwent late apoptosis/necrosis, which was close to the mortality rate (55.86%). The result indicated that the increase of mortality was related to the late apoptosis/necrosis. A similar result was reported by Wu *et al.* in 2010, who demonstrated that iron oxide nanoparticles were largely internalized in endothelial cells, and the uptake contributed to cell death by apoptosis.[7]

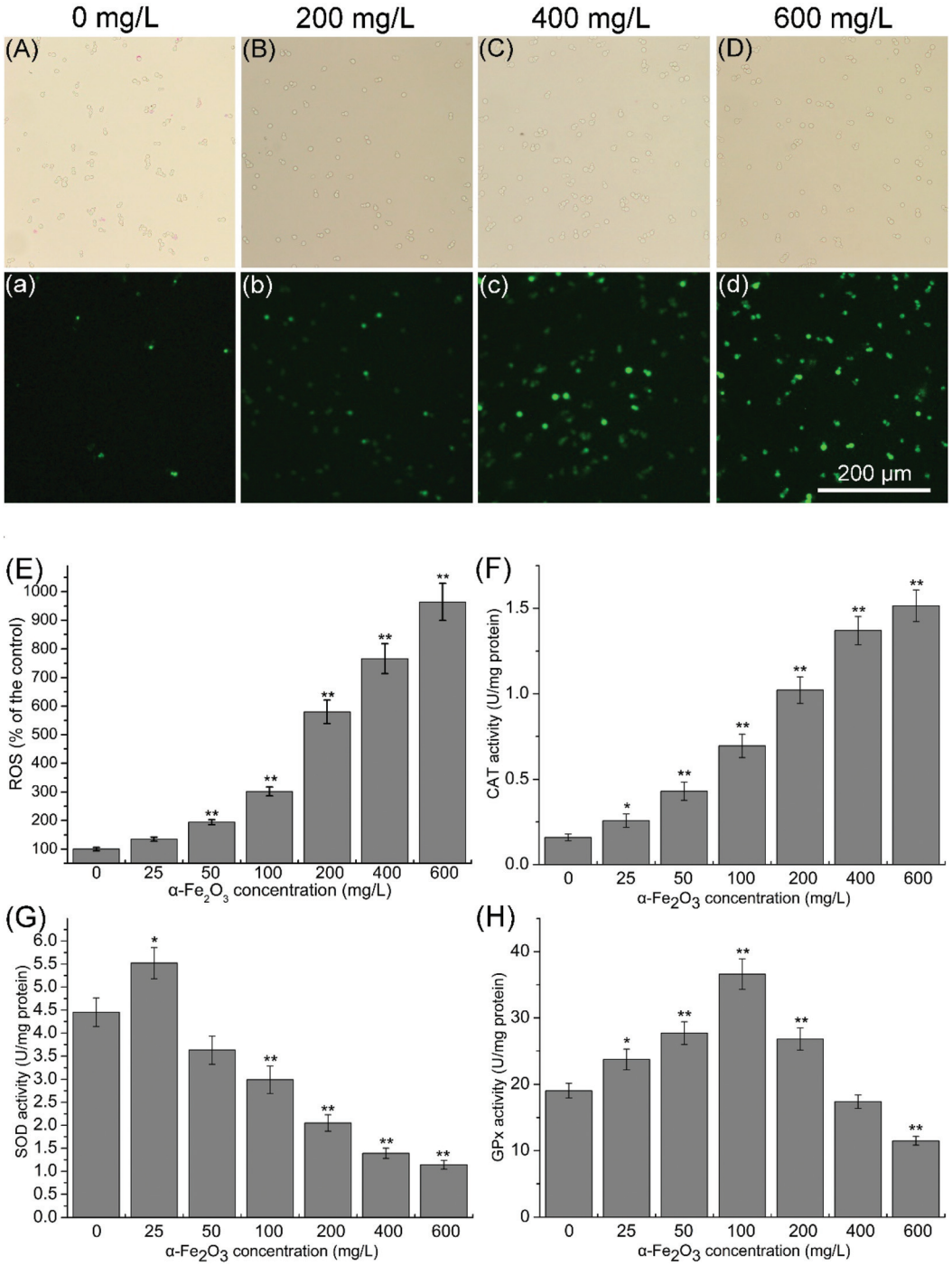

Fig. 6 Measurements of ROS and antioxidant enzyme activities. ROS generation of cells exposed to 0 (A and a), 200 (B and b), 400 (C and c) and 600 (D and d) mg L^{-1} α-Fe_2O_3-NP suspensions, and measured by using a fluorescence stereomicroscope. (E) ROS generation of cells exposed to 0–600 mg L^{-1} α-Fe_2O_3-NP suspensions, and measured by using a microplate reader. Effects of α-Fe_2O_3-NPs on CAT (F), SOD (G) and GPx (H) activities. Values are presented as mean ± SD. Values that are significantly different from the control are indicated by asterisks (one-way ANOVA, *$p < 0.05$, **$p < 0.01$).

3.5 MTP measurement

Reduction of MTP is an early step in the apoptotic process.[37] As shown in Fig. 5, MTP was observably decreased as indicated by the stronger green fluorescence (multimeric status) and weaker red fluorescence (monomeric status) with the α-Fe_2O_3-NP concentration increase from 0 to 600 mg L^{-1} (Fig. 5A, a1, a2: 0 mg L^{-1}; Fig. 5B, b1, b2: 200 mg L^{-1}; Fig. 5C, c1, c2: 400 mg L^{-1}; Fig. 5D, d1, d2: 600 mg L^{-1}). MTP was significantly decreased ($p < 0.01$) at 50–600 mg L^{-1} compared with the control (Fig. 5E), indicating that the apoptosis induced by α-Fe_2O_3-NPs was related to mitochondrial impairment. The decrease of MTP may be caused by the accumulated α-Fe_2O_3-NPs in the cytoplasm. The accumulated NPs have the potential to disturb the membranes of mitochondria, causing damage to them and inducing oxidative stress.[38] Moreover, internalized nanoparticles continuously release metal ions that will lead to mitochondrial dysfunction and ROS generation.[13]

3.6 Measurements of ROS and antioxidant enzyme activities

As described above, the accumulated NPs have the potential to induce oxidative stress. ROS, SOD, CAT and GPx are biomarkers of oxidative stress.[6,25,31] Production of ROS is a key cellular event of apoptosis in yeasts.[21,22] Moreover, there is a close relationship between ROS production and mitochondrial impairment. Disruption of ROS balance can result in the mitochondrial structure injury. In addition, damage to the mitochondria can lead to increased ROS production.[39,40] Antioxidant enzymes (such as CAT, SOD and GPx) catalyze the decomposition of ROS and protect organisms from the adverse effects of oxidative stress.

As shown in Fig. 6A–D, ROS was increased as indicated by stronger green fluorescence with the α-Fe_2O_3-NP concentrations increase from 0 to 600 mg L^{-1} (Fig. 6A and a: 0 mg L^{-1}; Fig. 6B and b: 200 mg L^{-1}; Fig. 6C and c: 400 mg L^{-1}; Fig. 6D and d: 600 mg L^{-1}), and markedly increased ($p < 0.01$) at 50–600 mg L^{-1} (Fig. 6E). Similar to ROS, CAT activity also showed a dose-dependent increase and dramatically increased ($p < 0.01$) at 50–600 mg L^{-1} (Fig. 6F). Interestingly, SOD (Fig. 6G) and GPx (Fig. 6H) activities firstly increased and then decreased. The increase of SOD and GPx activities may be due to their responses to superoxides; high antioxidant enzyme activities can efficiently degrade superoxides. On the other hand, high concentrations of ROS can inhibit the antioxidant enzyme activities, so their activities may be inhibited by the elevated ROS level.[6,41] In general, these results indicated that the apoptosis and mitochondrial impairment induced by α-Fe_2O_3-NPs were related to oxidative stress. A similar conclusion was reported by Horie *et al.* in 2011, who demonstrated that the internalized nanoparticles may affect cells *via* increased ROS levels followed by dysfunction of mitochondria and apoptosis.[13]

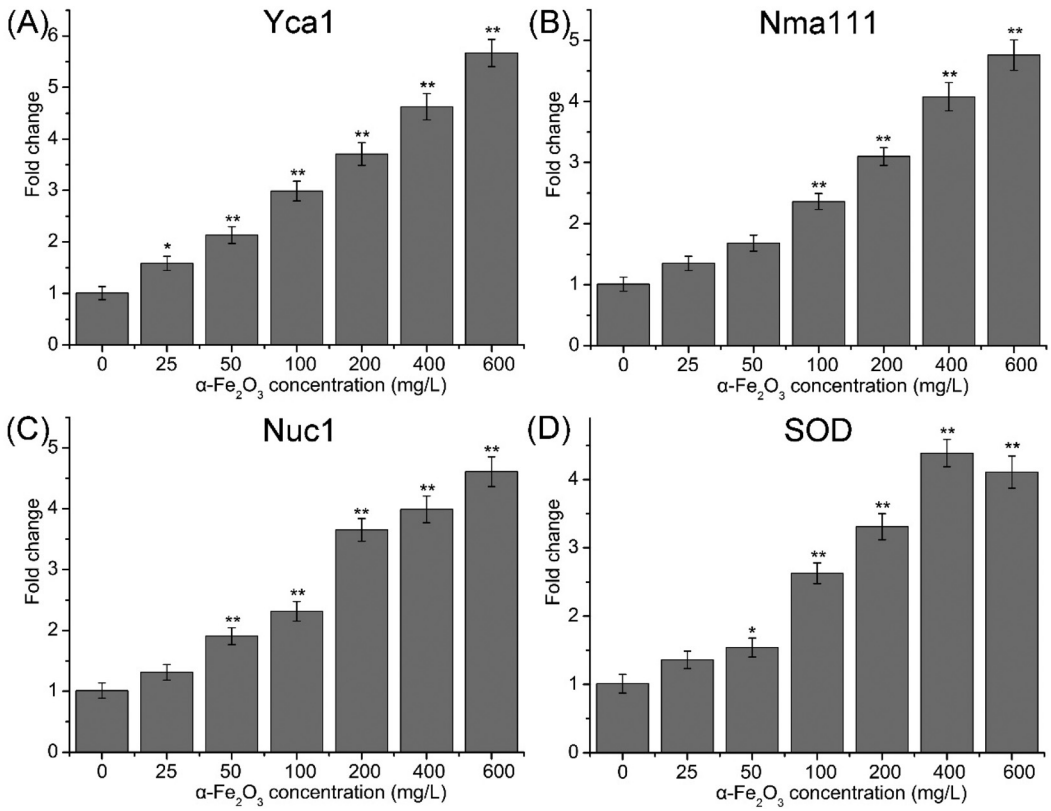

Fig. 7 Apoptosis-related mRNA expression in *S. cerevisiae* cells exposed to 0–600 mg L^{-1} α-Fe_2O_3-NP suspensions for 24 h. Values are presented as mean ± SD. Values that are significantly different from the controls are indicated by asterisks (one-way ANOVA, *$p < 0.05$; **$p < 0.01$).

3.7 Apoptosis-related mRNA expression

Yca1 belongs to the family of metacaspases that is found in yeasts, and regulates apoptosis.[42] Nma111p is a member of the HtrA family of serine proteases, and its overexpression enhances apoptotic cell death.[43] Nuc1p is a major mitochondrial nuclease, and plays vital roles in mitochondrial recombination and apoptosis.[44] SOD encodes superoxide dismutase and plays a key role in the redox reaction.[45] Furthermore, SOD also helps in protecting mitochondria from oxidative damage.[45] As shown in Fig. 7, expressions of Yca1, Nma111, Nuc1 and SOD were significantly increased ($p < 0.01$) at 100–600 mg L^{-1}, indicating that cells underwent apoptosis after exposure to α-Fe_2O_3-NPs. Besides, overexpression of Nuc1 and SOD implied that mitochondria were impaired following exposure.

4. Conclusion

In this study, the potential toxicity of α-Fe_2O_3-NPs to *S. cerevisiae* was investigated. The results so far showed that cell viability and proliferation were significantly decreased following exposure. Toxic effects were attributed to α-Fe_2O_3-NPs rather than iron ions released from the NPs, and related to apoptosis mediated by mitochondrial impairment and oxidative stress. This study mainly focused on the short-term effects of α-Fe_2O_3-NPs on *S. cerevisiae*, for safe and commercial purposes, chronic exposure to environmentally realistic concentrations should be performed in the further study.

Conflict of interest

There are no conflicts of interest to declare.

Acknowledgements

This work was supported by the Postdoctoral Science Foundation of Shaanxi Province (Program no. 2016BSHEDZZ114), the Special Funds for Talents in Northwest A&F University to B. Zhu (Program no. Z111021510) and the China Postdoctoral Science Foundation (Program no. 2015 M580888).

References

1 A. Predescu and A. Nicolae, Adsorption of Zn, Cu and Cd from waste waters by means of maghemite nanoparticles, *Upb Scientific Bulletin*, 2012, **74**, 255–264.
2 O. S. Wolfbeis, An overview of nanoparticles commonly used in fluorescent bioimaging, *Chem. Soc. Rev.*, 2015, **44**, 4743–4768.
3 X. L. Wu, Y. G. Guo, L. J. Wan and C. W. Hu, α-Fe_2O_3 Nanostructures: Inorganic Salt-Controlled Synthesis and Their Electrochemical Performance toward Lithium Storage, *J. Phys. Chem. C*, 2008, **112**, 16824–16829.
4 M. Alagiri and S. B. A. Hamid, Green synthesis of α-Fe_2O_3 nanoparticles for photocatalytic application, *J. Mater. Sci.: Mater. Electron.*, 2014, **25**, 3572–3577.
5 S.-W. Cao, Y.-J. Zhu, M.-Y. Ma, L. Li and L. Zhang, Hierarchically nanostructured magnetic hollow spheres of Fe_3O_4 and γ-Fe_2O_3: preparation and potential application in drug delivery, *J. Phys. Chem. C*, 2008, **112**, 1851–1856.
6 M. Radu, M. C. Munteanu, S. Petrache, A. I. Serban, D. Dinu, A. Hermenean, C. Sima and A. Dinischiotu, Depletion of intracellular glutathione and increased lipid peroxidation mediate cytotoxicity of hematite nanoparticles in MRC-5 cells, *Acta Biochim. Pol.*, 2010, **57**, 355–360.
7 X. Wu, Y. Tan, H. Mao and M. Zhang, Toxic effects of iron oxide nanoparticles on human umbilical vein endothelial cells, *Int. J. Nanomed.*, 2010, **5**, 385.
8 K. Kasemets, A. Ivask, H. C. Dubourguier and A. Kahru, Toxicity of nanoparticles of ZnO, CuO and TiO_2 to yeast *Saccharomyces cerevisiae*, *Toxicol. in Vitro*, 2009, **23**, 1116.
9 J. S. Kim, T.-J. Yoon, K. N. Yu, B. G. Kim, S. J. Park, H. W. Kim, K. H. Lee, S. B. Park, J.-K. Lee and M. H. Cho, Toxicity and tissue distribution of magnetic nanoparticles in mice, *Toxicol. Sci.*, 2006, **89**, 338–347.
10 S. Besnaci, S. Bensoltane, F. M. H. Braia, L. Zerari, S. Khadri and H. Loucif, Embryotoxicity evaluation of iron oxide Fe_2O_3 on land snails: Helix aspersa, *J. Entomol. Zool. Stud*, 2016, **4**, 317–323.
11 L. Sadeghi, B. V. Yousefi and H. Espanani, Toxic effects of the Fe_2O_3 nanoparticles on the liver and lung tissue, *Bratisl. Lek. Listy*, 2014, **116**, 373–378.
12 M. Ahamed, M. J. Akhtar, M. A. Siddiqui, J. Ahmad, J. Musarrat, A. A. Al-Khedhairy, M. S. Alsalhi and S. A. Alrokayan, Oxidative stress mediated apoptosis induced by nickel ferrite nanoparticles in cultured A549 cells, *Toxicology*, 2011, **283**, 101–108.
13 M. Horie, H. Kato, K. Fujita, S. Endoh and H. Iwahashi, In vitro evaluation of cellular response induced by manufactured nanoparticles, *Chem. Res. Toxicol.*, 2011, **25**, 605–619.
14 L. Otero-González, C. García-Saucedo, J. A. Field and R. Sierra-Álvarez, Toxicity of TiO_2, ZrO_2, Fe^0, Fe_2O_3, and Mn_2O_3 nanoparticles to the yeast, *Saccharomyces cerevisiae*, *Chemosphere*, 2013, **93**, 1201–1206.
15 C. Pimentel, S. M. Caetano, R. Menezes, I. Figueira, C. N. Santos, R. B. Ferreira, M. A. Santos and C. Rodrigues-Pousada, Yap1 mediates tolerance to cobalt toxicity in the yeast *Saccharomyces cerevisiae*, *Biochim. Biophys. Acta*, 2014, **1840**, 1977–1986.
16 E. N. Gromozova and S. I. Voychuk, *Influence of Radiofrequency Emf on the Yeast Sacharomyces Cerevisiae as Model Eukaryotic System*, Springer, US, 2007, vol. 22, pp. 167–175.
17 A. Goffeau, Four years of post-genomic life with 6000 yeast genes, *FEBS Lett.*, 2000, **480**, 37–41.
18 S. Grossetête, B. Labedan and O. Lespinet, FUNGIpath: a tool to assess fungal metabolic pathways predicted by orthology, *BMC Genomics*, 2010, **11**, 81.

19 W. H. Mager and J. Winderickx, Yeast as a model for medical and medicinal research, *Trends Pharmacol. Sci.*, 2005, **26**, 265–273.
20 D. J. Jamieson, Oxidative stress responses of the yeast *Saccharomyces cerevisiae*, *Yeast*, 1998, **14**, 1511.
21 F. Madeo, E. Fröhlich, M. Ligr, M. Grey, S. J. Sigrist, D. H. Wolf and K.-U. Fröhlich, Oxygen stress: a regulator of apoptosis in yeast, *J. Cell Biol.*, 1999, **145**, 757–767.
22 F. Madeo, E. Herker, S. Wissing, H. Jungwirth, T. Eisenberg and K. U. Fröhlich, Apoptosis in yeast, *Curr. Opin. Microbiol.*, 2004, **7**, 655–660.
23 N. Bayat, K. Rajapakse, R. Marinseklogar, D. Drobne and S. Cristobal, The effects of engineered nanoparticles on the cellular structure and growth of *Saccharomyces cerevisiae*, *Nanotoxicology*, 2014, **8**, 363–373.
24 S. Zhu, B. Zhu, A. Huang, Y. Hu, G. Wang and F. Ling, Toxicological effects of multi-walled carbon nanotubes on *Saccharomyces cerevisiae*: The uptake kinetics and mechanisms and the toxic responses, *J. Hazard. Mater.*, 2016, **318**, 650–662.
25 S. Zhu, F. Luo, W. Chen, B. Zhu and G. Wang, Toxicity evaluation of graphene oxide on cysts and three larval stages of *Artemia salina*, *Sci. Total Environ.*, 2017, **595**, 101–109.
26 S. Rhiem, M. J. Riding, W. Baumgartner, F. L. Martin, K. T. Semple, K. C. Jones, A. Schäffer and H. M. Maes, Interactions of multiwalled carbon nanotubes with algal cells: Quantification of association, visualization of uptake, and measurement of alterations in the composition of cells, *Environ. Pollut.*, 2015, **196**, 431–439.
27 P. Ludovico, M. J. Sousa, M. T. Silva, C. Leão and M. Côrtereal, *Saccharomyces cerevisiae* commits to a programmed cell death process in response to acetic acid, *Microbiology*, 2001, **147**, 2409.
28 I. Vermes, C. Haanen, H. Steffensnakken and C. Reutelingsperger, A novel assay for apoptosis. Flow cytometric detection of phosphatidylserine expression on early apoptotic cells using fluorescein labelled Annexin V, *J. Immunol. Methods*, 1995, **184**, 39–51.
29 E. Cavalieri, A. Rigo, M. Bonifacio, A. C. D. Prati, E. Guardalben, C. Bergamini, R. Fato, G. Pizzolo, H. Suzuki and F. Vinante, Pro-apoptotic activity of α-bisabolol in preclinical models of primary human acute leukemia cells, *J. Transl. Med.*, 2011, **9**, 45.
30 Y. Pan, A. Leifert, D. Ruau, S. Neuss, J. Bornemann, G. Schmid, W. Brandau, U. Simon and W. Jahnen-Dechent, Gold nanoparticles of diameter 1.4 nm trigger necrosis by oxidative stress and mitochondrial damage, *Small*, 2009, **5**, 2067–2076.
31 S. Zhu, F. Luo, B. Zhu and G.-X. Wang, Toxicological effects of graphene oxide on Saccharomyces cerevisiae, *Toxicol. Res.*, 2017, **6**, 535–543.
32 H. L. Karlsson, J. Gustafsson, P. Cronholm and L. Möller, Size-dependent toxicity of metal oxide particles–a comparison between nano- and micrometer size, *Toxicol. Lett.*, 2009, **188**, 112.
33 J. H. Lee, J. E. Ju, B. I. Kim, P. J. Pak, E. K. Choi, H. S. Lee and N. Chung, Rod-shaped iron oxide nanoparticles are more toxic than sphere-shaped nanoparticles to murine macrophage cells, *Environ. Toxicol. Chem.*, 2014, **33**, 2759–2766.
34 R. Suresh, L. Vijayalakshmi, A. Stephen and V. Narayanan, Hydrothermal Synthesis and Characterization of Cobalt Doped α-Fe_2O_3, *American Institute of Physics*, 2010, 362–367.
35 C. Wu, P. Yin, X. Zhu, C. Ouyang and Y. Xie, Synthesis of hematite (alpha-Fe_2O_3) nanorods: diameter-size and shape effects on their applications in magnetism, lithium ion battery, and gas sensors, *J. Phys. Chem. B*, 2006, **110**, 17806.
36 B. Ahmmad, K. Leonard, M. S. Islam, J. Kurawaki, M. Muruganandham, T. Ohkubo and Y. Kuroda, Green synthesis of mesoporous hematite (α-Fe_2O_3) nanoparticles and their photocatalytic activity, *Adv. Powder Technol.*, 2013, **24**, 160–167.
37 N. Zamzami, P. Marchetti, M. Castedo, C. Zanin, J.-L. Vayssiere, P. X. Petit and G. Kroemer, Reduction in mitochondrial potential constitutes an early irreversible step of programmed lymphocyte death in vivo, *J. Exp. Med.*, 1995, **181**, 1661–1672.
38 B. A. Katsnelson, L. I. Privalova, S. V. Kuzmin, V. B. Gurvich, M. P. Sutunkova, E. P. Kireyeva and I. A. Minigalieva, An Approach to Tentative Reference Levels Setting for Nanoparticles in the Workroom Air Based on Comparing Their Toxicity with That of Their Micrometric Counterparts: A Case Study of Iron Oxide Fe_3O_4, *Nanotechnology*, 2012, **12**, 1–13.
39 J. Li, X. Liu, Y. Zhang, F. Tian, G. Zhao, Q. Yu, F. Jiang and Y. Liu, Toxicity of nano zinc oxide to mitochondria, *Toxicol. Res.*, 2012, **1**, 137–144.
40 K. N. Yu, T. J. Yoon, A. Minaitehrani, J. E. Kim, S. J. Park, M. S. Jeong, S. W. Ha, J. K. Lee, J. S. Kim and M. H. Cho, Zinc oxide nanoparticle induced autophagic cell death and mitochondrial damage via reactive oxygen species generation, *Toxicol. in Vitro*, 2013, **27**, 1187–1195.
41 I. Oncel, E. Yurdakulol, Y. L. Kurt and A. Yildiz, Role of antioxidant defense system and biochemical adaptation on stress tolerance of high mountain and steppe plants, *Acta Oecol.*, 2004, **26**, 211–218.
42 F. Madeo, E. Herker, C. Maldener, S. Wissing, S. Lächelt, M. Herlan, M. Fehr, K. Lauber, S. J. Sigrist and S. Wesselborg, A Caspase-Related Protease Regulates Apoptosis in Yeast, *Mol. Cell*, 2002, **9**, 911–917.
43 B. Fahrenkrog, U. Sauder and U. Aebi, The S. cerevisiae HtrA-like protein Nma111p is a nuclear serine protease that mediates yeast apoptosis, *J. Cell Sci.*, 2004, **117**, 115–126.
44 S. Büttner, T. Eisenberg, D. Carmonagutierrez, D. Ruli, H. Knauer, C. Ruckenstuhl, C. Sigrist, S. Wissing, M. Kollroser and K. U. Fröhlich, Endonuclease G Regulates Budding Yeast Life and Death, *Mol. Cell*, 2007, **25**, 233.
45 L. A. Sturtz, K. Diekert, L. T. Jensen, R. Lill and V. C. Culotta, A Fraction of Yeast Cu,Zn-Superoxide Dismutase and Its Metallochaperone, CCS, Localize to the Intermembrane Space of Mitochondria A Physiological Role For SOD1 in Guarding Against Mitochondrial Oxidative Damage, *J. Biol. Chem.*, 2001, **276**, 38084–38089.

